Science of the Total Environment 541 (2016) 920–927

Contents lists available at ScienceDirect

Science of the Total Environment

journal homepage: www.elsevier.com/locate/scitotenv

Roadside vegetation barrier designs to mitigate near-road air pollution impacts

Zheming Tong [a,1], Richard W. Baldauf [b,c], Vlad Isakov [c], Parikshit Deshmukh [d], K. Max Zhang [a,*]

[a] Sibley School of Mechanical and Aerospace Engineering, Cornell University, Ithaca, NY, USA
[b] U.S. Environmental Protection Agency, Office of Research and Development, Research Triangle Park, NC, USA
[c] U.S. Environmental Protection Agency, Office of Transportation and Air Quality, Ann Arbor, MI, USA
[d] Jacobs Technologies, 109 TW Alexander Drive, Durham, NC 27713, USA

HIGHLIGHTS

- We studied effects of roadside barrier designs on near-road particle concentrations.
- Wide and dense vegetation barriers are a viable design option.
- Vegetation barriers planted next to solid barriers are another viable option.
- The effects of vegetation barriers are particle size-dependent.
- The degree of on-road concentration increase varies with wind direction.

GRAPHICAL ABSTRACT

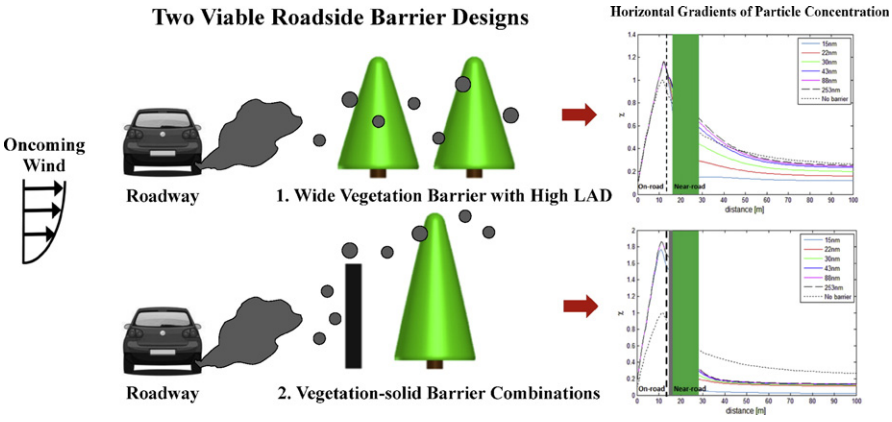

ARTICLE INFO

Article history:
Received 29 June 2015
Received in revised form 12 September 2015
Accepted 14 September 2015
Available online 9 October 2015

Editor: D. Barcelo

Keywords:
CFD
Particulate matter (PM)
Ultrafine particle (UFP)
Urban planning
Green infrastructure
Dry deposition
Air quality

ABSTRACT

With increasing evidence that exposures to air pollution near large roadways increases risks of a number of adverse human health effects, identifying methods to reduce these exposures has become a public health priority. Roadside vegetation barriers have shown the potential to reduce near-road air pollution concentrations; however, the characteristics of these barriers needed to ensure pollution reductions are not well understood. Designing vegetation barriers to mitigate near-road air pollution requires a mechanistic understanding of how barrier configurations affect the transport of traffic-related air pollutants. We first evaluated the performance of the Comprehensive Turbulent Aerosol Dynamics and Gas Chemistry (CTAG) model with Large Eddy Simulation (LES) to capture the effects of vegetation barriers on near-road air quality, compared against field data. Next, CTAG with LES was employed to explore the effects of six conceptual roadside vegetation/solid barrier configurations on near-road size-resolved particle concentrations, governed by dispersion and deposition. Two potentially viable design options are revealed: a) a wide vegetation barrier with high Leaf Area Density (LAD), and b) vegetation–solid barrier combinations, i.e., planting trees next to a solid barrier. Both designs reduce downwind particle concentrations significantly. The findings presented in the study will assist urban planning and forestry organizations with evaluating different green infrastructure design options.

* Corresponding author.
E-mail address: kz33@cornell.edu (K. Max Zhang).
[1] Now at Center for Green Buildings and Cities, Graduate School of Design, Harvard University, Cambridge, MA, 02138.

http://dx.doi.org/10.1016/j.scitotenv.2015.09.067
0048-9697/

1. Introduction

Roadside vegetation barriers have been evaluated as a potential mitigation strategy for near-road air pollution in several field, wind tunnel, and numerical studies (Al-Dabbous and Kumar, 2014; Baldauf et al., 2008; Bowker et al., 2007; Brantley et al., 2014; Hagler et al., 2012; Heist et al., 2009; Finn et al., 2010; Steffens et al., 2012, 2013, 2014). Those studies revealed that the effects of vegetation barriers on near-road air quality are primarily governed by two physical mechanisms: dispersion and deposition (Steffens et al., 2012, 2013, 2014). The impact of dispersion is demonstrated by upward deflection and deceleration of the approaching air flow from the highway, as well as flow recirculation on both sides of the barrier. Deposition, on the other hand, removes particulate matter (PM) by Brownian diffusion, impaction, interception and gravitational settling. The deposition velocity, V_d, varies considerably depending on the particle size, for example, from ~3 cm s^{-1} for 20 nm particles to ~0.3 cm s^{-1} for particles at approximately 100 nm (Zhang et al., 2001). Steffens et al. (2012) simulated the effects of vegetation barriers on near-road particle size distributions characterized by a field experiment, and examined the knowledge gaps in capturing the impacts of dispersion and deposition, as well as proposed several recommendations on how to bridge those gaps.

The main objective of this study is to advance our understanding of the effectiveness of vegetation barriers as a potential mitigation strategy by quantitatively assessing the spatial variation of PM under various road-canopy configurations commonly present in the real world. We first incorporated the Large Eddy Simulation (LES) turbulence model, as recommended by Steffens et al. (2012), into the Comprehensive Turbulent Aerosol Dynamics and Gas Chemistry (CTAG) model, and evaluated the model performance against the same experimental dataset adopted by Steffens et al. (2012), which employed a Reynolds Averaged Navier–Stokes (RANS) turbulence model. Next, we compared six common near-road vegetation barrier configurations in terms of their impact to on-road and near-road particle concentrations. Finally, we provided design recommendations based on the results of our analysis.

2. Numerical method

The CTAG model was designed to resolve the flow field, including turbulent reacting flows, aerosol dynamics, and gas chemistry in complex environments (Steffens et al., 2013; Tong et al., 2012; Tong and Zhang, 2015; Wang and Zhang, 2009, 2012; Wang et al., 2011, 2013a, 2013b). In this study, Large Eddy Simulation (LES) is applied to resolve the large-scale dominant unsteady motion within the vegetation canopy and requires modeling only small-scale, unresolvable turbulent motions. Previous studies demonstrated that LES is capable of reproducing many observed features of turbulent flow within vegetation canopies by comparing with field and wind tunnel observations (Dupont and Brunet, 2008; Shaw and Schumann, 1992; Su et al., 1998). Steffens et al. (2013) compared the performances of LES and RANS models in predicting the spatial variations of tracer species behind a solid barrier, which demonstrated LES' advantages in resolving the flow recirculation patterns that commonly exist in the presence of a barrier.

2.1. Spatial averaging of vegetation

Vegetation consists of numerous irregular small leaf and branch structures that inhibit the motion of incoming air flow. This complex structure within plant canopies makes it computationally prohibitive for explicit numerical modeling. In order to overcome this obstacle, the vegetation is spatially averaged to generate average flow speed and turbulence statistics within the canopy (Wilson and Shaw, 1977). The canopy is represented by a region of fluid only, where branches and leaves are not physically modeled. Their effects are modeled as sink terms in the governing equations (Sections 2.2 and 2.3). Detailed assumptions on spatial averaging practice are described in Steffens et al. (2012).

2.2. Large Eddy Simulation (LES)

LES with a dynamic subgrid model is modified to include the aerodynamic effects of the drag element due to leaf and branch structures that impede the motion of incoming flow (Shaw and Schumann, 1992; Dupont and Brunet, 2008). In LES, filtered continuity and momentum equations are shown below:

$$\frac{\partial \rho}{\partial t} + \frac{\partial \rho \tilde{u}_j}{\partial x_j} = 0 \tag{1}$$

$$\frac{\partial \rho \tilde{u}_i}{\partial t} + \frac{\partial \rho \tilde{u}_i \tilde{u}_j}{\partial x_j} = -\frac{\partial \tilde{p}}{\partial x_i} + \frac{\partial \tau_{ij}}{\partial x_j} + \frac{\partial \sigma_{ij}}{\partial x_j} + S_u. \tag{2}$$

S_u is a drag term imposed by the vegetation, which is proportional to the Leaf Area Density (LAD) and the plant drag coefficient shown in Eq. (3) (Thom, 1972):

$$S_u = -\rho C_D LAD u^2 \tag{3}$$

τ_{ij} is the filtered stress tensor, and σ_{ij} is the subgrid-scale Reynolds stress, which is modeled by the Boussinesq hypothesis in Eq. (4):

$$\sigma_{ij} - \frac{1}{3}\delta_{ij}\sigma_{kk} = -2\mu_t \overline{S_{ij}}. \tag{4}$$

$\overline{S_{ij}}$ is the rate of strain tensor of the resolved scale under the presence of the vegetation drag term. A well-established dynamic Smagorinsky model shown in Eq. (5) is employed to model the subgrid viscosity μ_t in Eq. (4) (Germano et al., 1991). The dynamic model removes some problems associated with the constant coefficient Smagorinsky model by eliminating the need to prescribe a length scale and near-wall correction (Pope, 2000).

$$\mu_t = \rho (L_S)^2 |\overline{S}| \tag{5}$$

L_s is the mixing length scale that depends on the size of the computational cell and the dynamically-computed Smagorinsky constant.

Researchers in the past either modeled the subgrid viscosity by solving an additional kinetic energy transport equation with a source term to represent the creation of turbulent kinetic energy (TKE) by vegetation, or directly employed the dynamic Smagorinsky model (Cassiani et al., 2008; Shaw and Zhang, 1992; Watanabe, 2004). In this study, we compared the two subgrid modeling approaches. As illustrated in the Supporting Information, the performance is very similar, likely due to the fact that the majority of the TKE is explicitly resolved, and only a small portion is modeled. We therefore choose the dynamic Smagorinsky model for the purpose of lower computational cost.

2.3. Particle dispersion and deposition

Only dispersion and deposition are considered in the model. Any process that leads to particle transformation is not explicitly simulated, which is a limitation in our modeling approach. However, by constraining the emission factors against the data at the no-barrier site, we have equivalently incorporated the aerosol dynamics from roadway to the barrier site. More details are provided in Section 3.2. A scalar transport equation is employed to model particle dispersion and

deposition from on and near roadways:

$$\frac{\partial \widetilde{N_p(D_P)}}{\partial t} + \frac{d\widetilde{u}_j \widetilde{N_p(D_P)}}{dx_j} = \frac{\partial}{\partial x_j}\left[(D_t + D_m)\frac{\partial \widetilde{N_p(D_P)}}{\partial x_j}\right] + S_d(D_P). \quad (6)$$

$\widetilde{N_p(D_P)}$ is the average particle concentration for each particle size. D_t is the turbulent diffusivity, and D_m is the molecular diffusivity. S_d is the sink term to represent the effect of deposition, which is the function of particle size D_P.

$$S_d(D_p) = \widetilde{N_p(D_P)}\, V_d(D_P) LAD \quad (7)$$

$V_d(D_p)$ is the particle deposition velocity, and in this study we adopt the dry deposition model from Zhang et al. (2001). Note that the aerodynamics resistance r_a (part of the total resistance to compute deposition velocity) is not included since the aerodynamic effect is already explicitly resolved by LES.

3. Model evaluation

3.1. Chapel Hill field experiment

The CTAG with LES model for vegetation barriers is evaluated against experimental data collected in Chapel Hill, North Carolina, USA as reported by Hagler et al. (2012). For this study, the near-road vegetation barrier consisted of a mix of 6–9 m tall coniferous trees with full cover from the ground to the top of the canopy. A section along the same stretch of limited-access roadway contained the roadside vegetation barrier as well as an area with no barrier or other obstructions to air flow from the road. Wind speed and direction measurements were collected using a 3-D ultrasonic anemometer with a sampling frequency of 1 Hz. Particle size distributions (PSD) were obtained using scanning mobility particle sizers (SMPS), which captured 88 size channels ranging from 12.6 nm to 289 nm both at the no-barrier site and behind the barrier at two heights.

3.2. Boundary conditions

In the Chapel Hill simulation, the computational domain and boundary condition are identical to those in our previous paper (Steffens et al., 2012). The computational domain and satellite image can be found in the Supporting Information. The inlet profile and vehicle-induced turbulence (VIT) are constrained in the way that modeled wind velocity matches the measured values at the no-barrier site. The traffic emission factor cannot be determined experimentally; therefore, the road-level, size-resolved emission factors (Zhang et al., 2005) were derived based on PSD measurements at the no-barrier site using inverse modeling. In other words, the PSD of vehicular emissions released from traffic on the road is set such that PSD simulated at the no-barrier site matches that of the experiment. The road-level emission factor, which describes the emission profiles on or near the roadway curb, takes into account any changes in PSD due to particle transformation in the "tailpipe-to-road" process (Zhang and Wexler, 2002). The friction velocity is estimated by matching the velocity profile at the top of the canopy (Stull, 1988; Steffens et al., 2012). Additional details can be found in Steffens et al. (2012).

3.3. Simulation results

Three periods were selected according to the description in Steffens et al (2012), namely Morning, Peak 1, and Peak 2, as the wind speed and direction are relatively constant among the three periods (Steffens et al., 2012). In this model, nine discrete bins were employed to represent the PSD from 12.6 nm to 289 nm. The Leaf Area Density (LAD) profile of the vegetation barrier is set the same as Steffens et al. (2012). Fig. 1 illustrates the simulation results for the three selected scenarios.

As shown in Fig. 1, although discrepancies are present, the CTAG with LES model adequately captures the trend observed in the experiment. The model prediction shows close agreement with on-site measurements behind the vegetation barrier. The differences are likely due to spatial averaging of modeled vegetation and uncertainties in data collection, which cannot fully simulate branches and leaves in reality.

4. Evaluation of vegetation barrier design configurations

4.1. Barrier configurations

Six common near-road configurations, as well as a series of sensitivity studies on several physical parameters, are investigated in this section (Table 1, Fig. 2). The evaluated LES model is employed to simulate near-road PSDs. Table 1 shows the physical parameters of the barrier and boundary conditions studied. The composition of the canopy structure is modeled using two plant parameters widely used in the literature, Leaf Area Density (LAD) and Leaf Area Index (LAI). LAD is a ratio of leaf surface area to total volume occupied by vegetative element whereas LAI measures the ratio of the leaf surface area to ground surface area. LAD profiles for all configurations are obtained from Steffens et al. (2012) based on LAI measurement with a LAI-2000 plant canopy analyzer (Hagler et al., 2012), representing coniferous evergreens, which are usually preferable in air pollution mitigation because of their high surface areas, low VOC emission rates, limited seasonal changes, and long lives (Fuller et al., 2009; Lovett, 1994; McDonald et al., 2007). The

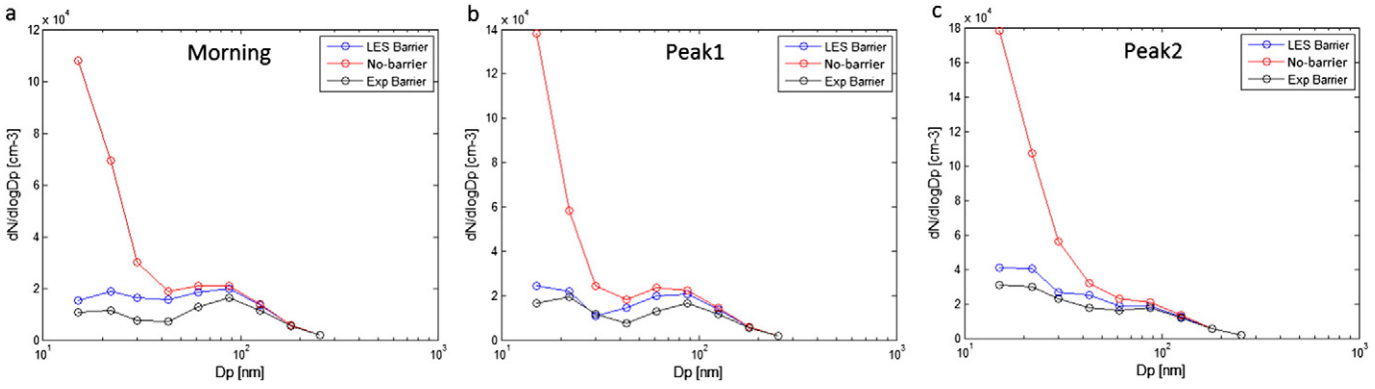

Fig. 1. Particle size distributions (PSD) for three modeling scenarios (Morning, Peak 1, Peak 2). "LES Barrier" stands for simulation results by Large Eddy Simulation (LES). "No-barrier" stands for experimental result at the no-barrier site. "Exp Barrier" stands for the experimental result behind the barrier. The measured PSDs are those with background (i.e., upwind) values subtracted.

Table 1
Description of roadside barrier geometry for all configurations tested.

Case #	0	1	2	3[a]	4		5	
					Solid barrier	Vegetation barrier	Upwind vegetation barrier	Downwind vegetation barrier
Height	N/A	6 m, 9 m	6 m	6 m	6 m	10 m	6 m	6 m
Width	N/A	6 m, 12 m, 18 m	1 m	1 + 0.25 m	1 m	6 m	6 m	12 m
LAD[b]	1	1,1.5	N/A	0.33[c]	N/A	1	1	1
U	2 m/s	1, 2, 4 m/s	2 m/s	2 m/s	2 m/s		2 m/s	
Stability[d]	Unstable	Stable, unstable, neutral	Unstable	Unstable	Unstable		Unstable	
Direction[e]	90°	90°	90°	90°	30°, 45°, 90°		90°	
Distance[f]	N/A	3 m, 20 m	3 m	3 m	3 m		3 m	

[a] Case 3 represents a solid barrier with vegetation cover. The thickness of the cover is 25 cm.
[b] LAD in the unit of m^2m^{-3}. "1" stands for the baseline LAD profile of conifer trees, "0.5" means 50% less of the baseline LAD, and "1.5" is 50% more than the baseline LAD.
[c] LAD = 0.33 m^2m^{-3} is calculated based on LAI = 2 for the vegetation cover assuming constant cover thickness.
[d] The unstable condition is defined with a negative Monin–Obukhov length L and a positive L for stable condition. L of the neutral condition is larger than 10^5 m.
[e] 90° represents the oncoming wind direction that is perpendicular to the road. 0° is parallel to the road.
[f] It is the distance between roadway and barrier.

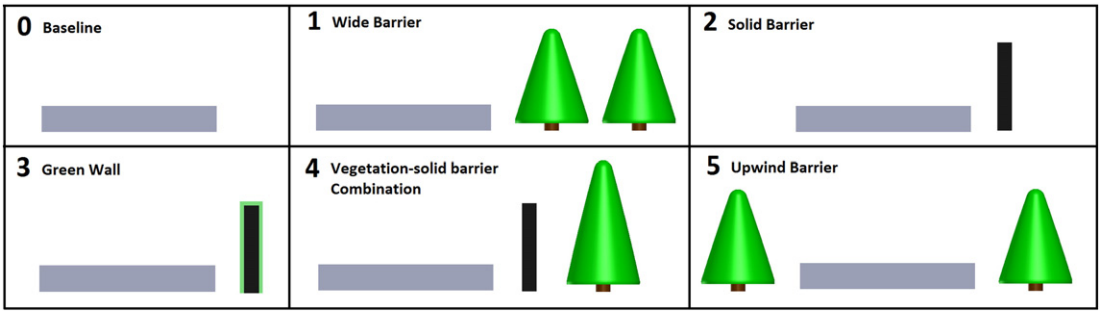

Fig. 2. The schematic of six roadside barrier configurations is shown in side view. In the simulation, the complex geometry of the vegetation canopy is modeled as rectangular blocks. Leaf Area Density (LAD) profile of coniferous trees is applied on each block to represent the real geometry of coniferous evergreen.

inlet wind profile for the baseline case is also taken from Steffens et al. (2012), representing unstable conditions. Wind direction is perpendicular to the roadway for most cases.

As presented in Table 1, Case 0 stands for a no-barrier scenario, which serves as a comparison for the other configurations. Case 1 is the configuration with a wide vegetation barrier located next to the road. Case 2 represents a solid barrier, and Case 3 represents a "green wall", which is a combination of solid barrier and vegetation cover. Leaf area index (LAI = 2) of the vegetation cover is taken from the literature (Litschke and Kuttler, 2008). Case 4 represents a scenario where a tall vegetation barrier is behind a solid wall, referred to as "vegetation–solid barrier combination". Case 5 represents a condition where both upwind and downwind vegetation barriers are present. The dimension of each configuration and simulation perimeters are also shown in Table 1.

4.2. Boundary conditions

For the six tested configurations, the computational domain has a dimension of 250 m × 200 m × 30–50 m divided into 3.5 to 5 million elements. The average element size of the vegetation barrier is about 0.3 m. The height of the domain is about 5 times the height of the barrier, which avoids blocking effects and unphysical flow acceleration (Tominaga et al., 2008). A grid independency study was conducted to ensure the results are independent of domain size and mesh resolution. The schematic drawing of the baseline configuration is shown in Fig. 3. The ground surface and solid barrier surfaces are defined as a no-slip wall. The top and two sides of the computational domain are set as symmetry conditions with zero shear. Outflow boundary condition is specified at the outlet of the domain. The average inlet wind velocity u is 2 m/s for the baseline. Wind direction is normal to the barrier except for Case 4 where we explored how the roadside air quality varies with wind direction. The vehicular size-resolved emission factor and VIT are set the same as those for the Chapel Hill case.

4.3. Results and discussion

4.3.1. Case 1

Fig. 4a shows the normalized horizontal gradients of particle concentration χ for diameters varying from 15 nm to 253 nm. χ is the particle concentration normalized by the peak concentration from the no-barrier case at the same particle size. The effects of the vegetation barriers are evident in three regimes: On-road, the immediate vicinity behind the vegetation barrier, and near-road.

For the on-road regime, the presence of a vegetation barrier elevates the on-road concentration due to the deceleration of the perpendicular wind and on-road particle accumulation upwind to the barrier. For this

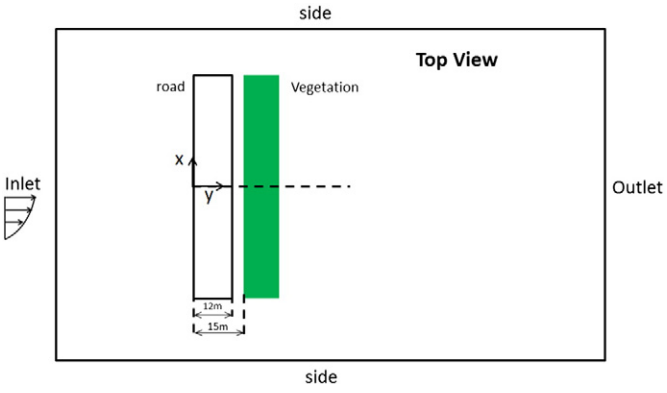

Fig. 3. Schematics of the baseline configuration (Case 1).

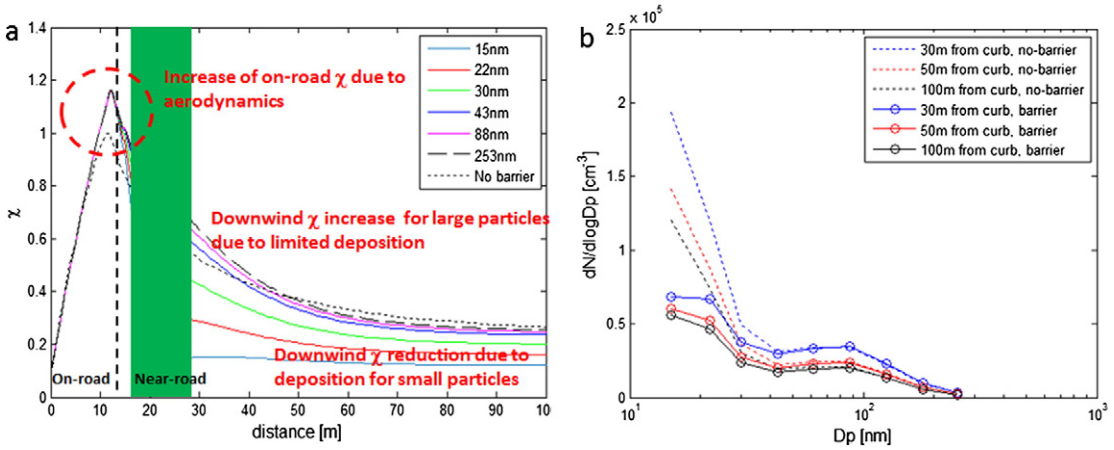

Fig. 4. a) Horizontal gradients of size-resolved particle concentrations from 15 nm to 253 nm in diameter. 9 particle sizes are simulated, but 6 bins are plotted for clarity. χ is the particle concentration normalized by the peak concentration from the no-barrier case at the same particle size. The vertical dash line separates the on-road and near-road domains. The green strip indicates the location and width of the vegetation barrier. b) Particle size distribution (PSD) of the baseline; dash lines represent the no-barrier case.

particular configuration, a roughly 15% increase over the no-barrier case is observed (Fig. 4a, b). This phenomenon is similar to that often observed in the literature of solid barriers (Baldauf et al., 2011; Hagler et al., 2011; Finn et al., 2010).

For the regime of the immediate vicinity behind the vegetation barrier (~20 m downwind of the barrier for this case), reduced dispersion within the vegetation canopy and the behind-barrier wake zone results in greater concentrations for relatively large particles with low deposition velocity than that of the no-barrier case, as the effects of dispersion in the no barrier section overwhelm the deposition for those particles within the vegetation. In contrast, a sharp drop in concentrations is observed for relatively small particles (<30 nm) with high deposition velocity (Fig 4a).

For the near-road regime (beyond ~20 m downwind of the barrier for this particular case), a lower concentration than that for the no-barrier case ocurrs for all particle sizes. A mass balance analysis is conducted for the 180 nm particles (with low deposition velocity). It is shown that the increase of the total particle number with vegetation over the no-barrier case is almost equivalent to the decrease of the total particle number over the same case. This implies that the on-road particle accumulation leads to near-road pollutant reduction when deposition is absent. Details for the mass balance analysis are presented in the Supporting Information.

4.3.2. Cases 2, 3 and 4

For the scenario with a roadside solid barrier (Case 2), a significant reduction behind the barrier is observed for all particle sizes as the plume is forced to deflect upward when approaching the barrier. Consistent with the findings from Steffens et al. (2013, 2014), the presence of a solid barrier creates an upward deflection of incoming airflow and a recirculation cavity behind, which increases the on-road particle concentrations but results in a concentration deficit across it (Fig. 5a). Fig. 5b shows that the horizontal gradients behind a solid barrier with vegetation cover (Case 3) are very similar to that behind a solid barrier (Case 2), which suggests that the additional particle reduction by having vegetation cover on solid barriers is insignificant because the total leaf surface area of vegetation cover is small in contrast with the tree stands and the boundary layer formed along the solid barrier surface likely inhibits air flow through the vegetation.

Case 4, i.e., "vegetation–solid barrier combination", sees the largest reduction in particle concentrations downwind of the barrier due to the synergistic effect between the solid barrier and vegetation canopy (Fig. 5c). Relative to Cases 2 and 3, the concentrations of all particle sizes are lower than for both the no-barrier case (Case 0) and the solid barrier case (Case 2) downwind of the barrier.

4.3.3. Case 5

The upwind vegetation barrier in Case 5 substantially elevates the on-road concentration over the no-barrier case since it slows down the on-road dispersion (Fig. 6) when the wind direction is normal to the barrier. However, a steeper concentration decline along the wind direction is found for all particle sizes compared with the no-barrier case. This ultimately results in lower concentration further downwind

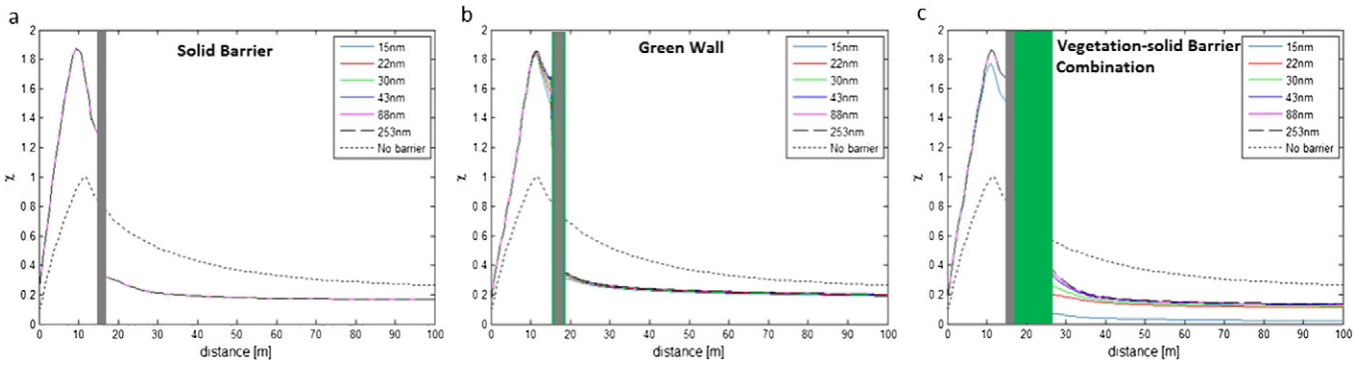

Fig. 5. Horizontal gradients of size-resolved particle concentrations for Cases 2 (a), 3 (b) and 4 (c). The green strip indicates the location and width of the vegetation barrier. The gray strip indicates the location and width of the solid barrier. The strips with green on both sides designate the location and width of a "green wall".

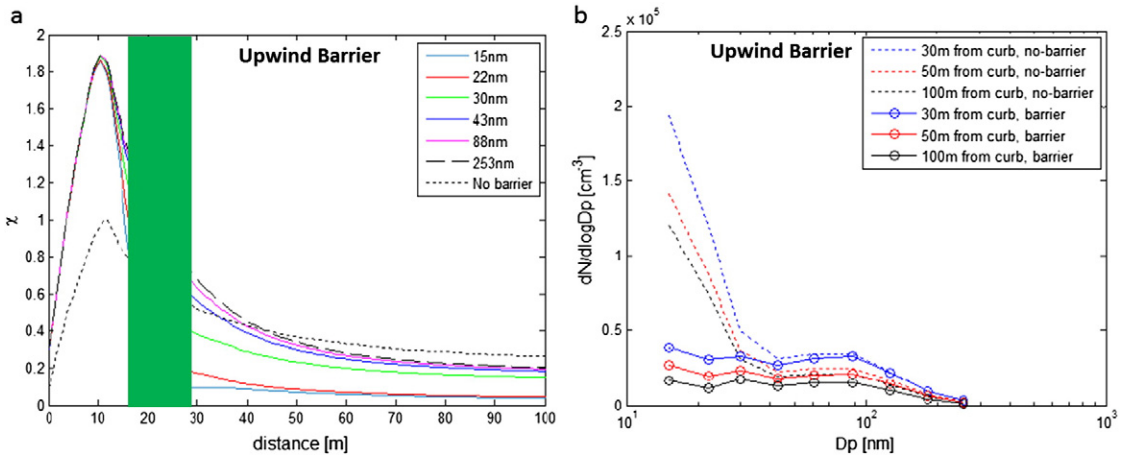

Fig. 6. a) Horizontal gradients of size-resolved particle concentrations for Case 5; b) Particle size distribution (PSD) for Case 5; the green area indicates the location and width of the vegetation barrier.

in the far field compared with those at the same distances downwind of the no-barrier case.

4.3.4. Sensitivity study

4.3.4.1. Leaf Area Density. LAD is an important parameter for determining the amount of deposition that takes place within the canopy as well as the reduction in air flow turbulence (Petroff et al., 2009). To test the effect of LAD, a sensitivity study is performed by increasing the baseline LAD by 50% while fixing the rest of the parameters. It is found that increasing LAD leads to substantially lower concentration behind the barrier than those from the baseline case, especially for particles ≤50 nm (Fig. 7a, b). However, this effect is non-linear suggesting that simply doubling the LAD will not double the reduction of the particle concentration. A noteworthy finding is illustrated in Fig. 7 where the PSD from the solid barrier case (Fig. 7c) is placed on the right end. For relatively large particles with low deposition velocity, increasing LAD leads to more concentration reduction beyond 30 m downwind of the canopy. The overlapping PSD curves in Fig. 7c result from absence of deposition for the solid barrier. In other words, the effects of solid barriers lead to more reduction for particles with small deposition velocity (i.e., large size) but less reduction for those with large deposition velocity (i.e., small size) than the equivalent cases for vegetation barriers.

4.3.4.2. Vegetation barrier width. The width of a vegetation barrier is another important factor for roadside dispersion and deposition (Brantley et al., 2014). The barrier width of Case 1 is varied by ±50% to test its sensitivity. Increasing the width of the vegetation barrier results in a greater concentration reduction behind the barrier for all particle sizes due to enhanced deposition effects of vegetation (Fig. 8). In addition, increasing the width of the vegetation barrier also likely raises on-road concentrations due to weakened on-road dispersion, but to a lesser extent than the cases with solid barriers.

4.3.4.3. Oblique wind direction. An increase of on-road concentration upwind of roadside barriers has been discussed in the literature as a result of blocking on-road dispersion (Baldauf et al., 2008; Heist et al., 2009; Hagler et al., 2011; Steffens et al., 2013). Case 4 is chosen as the baseline due to the largest on-road concentration elevation. A translational periodic boundary condition is applied on the sides as we model a section of roadway with finite length. Our simulation indicates that the degree of on-road increase is contingent on incoming wind direction (Fig. 9). The on-road concentration decreases with more parallel winds to the road due to reduced blocking of on-road dispersion.

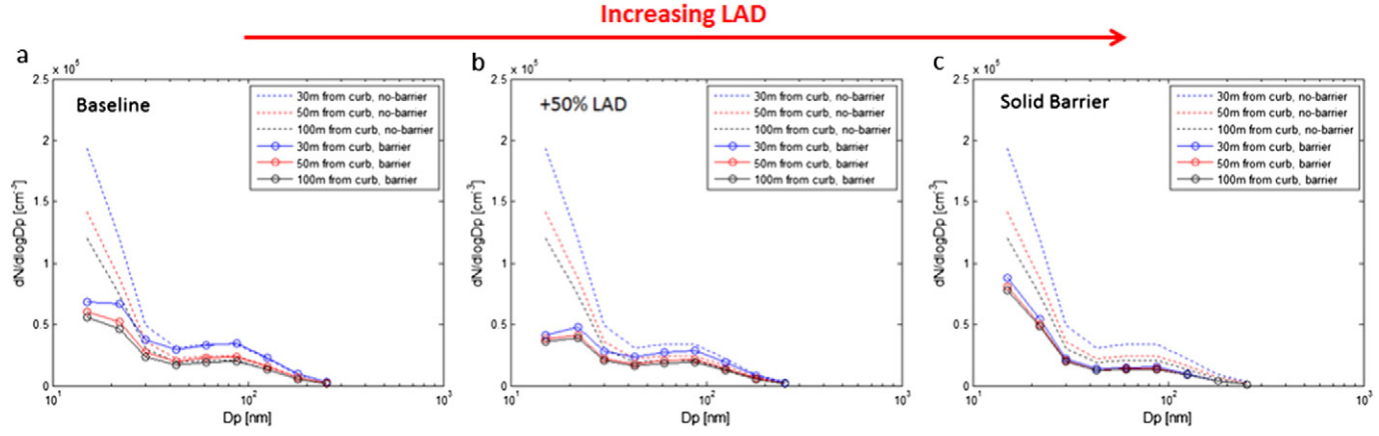

Fig. 7. PSDs with increasing LAD a) baseline LAD b) +50% LAD c) solid barrier.

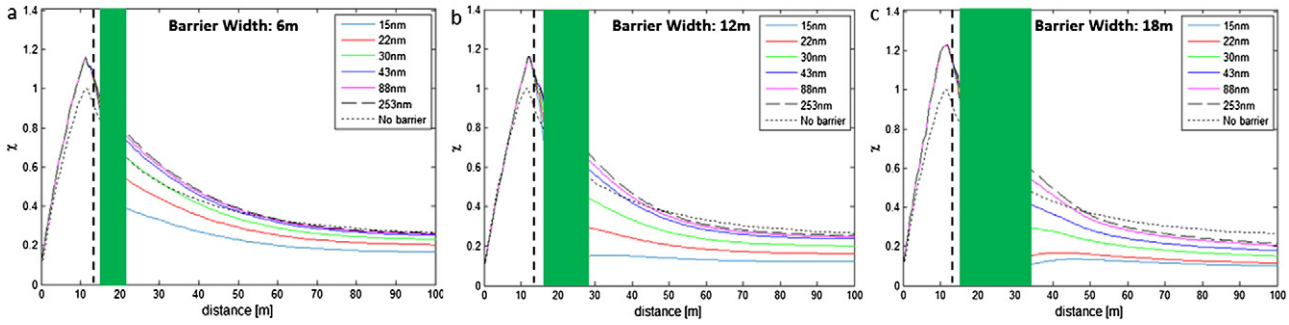

Fig. 8. Horizontal gradients of Case 1 with a) 6 m b) 12 m and c) 18 m vegetation barrier.

4.3.4.4. Barrier height and distance from roadway. The impact of the barrier height is investigated by increasing the baseline barrier height (6 m) by 50% to 9 m. The overall trends remain roughly the same as the baseline case. In addition, the increased barrier height slightly reduces the on-road dispersion by blocking the upward plume (Fig. S8b in the Supporting Information). The influence of the distance between the vegetation barriers and the road is also explored. Compared with the baseline case, the on-road particle concentrations decrease slightly due to less blocking effect (Fig. S8c in the Supporting Information). As the plume is first diluted over distance before reaching the barrier, the reduction for the concentrations of particles <30 nm due to deposition is less than that of the baseline case. More description can be found in the Supporting Information.

5. Conclusion

The primary objective of this study is to provide design recommendations to assist urban planners in evaluating different green infrastructure designs. The near-road air quality is primarily driven by two physical mechanisms, i.e., dispersion and deposition, and deposition only occurs in the presence of vegetation. Our analysis demonstrates that the impacts on roadside air quality are particle size-dependent. Two potentially viable design options with regard to roadside mitigation of near-road PM are revealed: a) a wide vegetation barrier with high Leaf Area Density (Case 1 with high LAD and width), and b) vegetation–solid barrier combinations, i.e., planting trees next to a solid barrier (Case 4).

A solid barrier (Case 2, Fig. 5a) creates an upward deflection of incoming airflow and deceleration of the approaching flow, which increases the on-road particle number concentration but results in a large concentration drop across it. In this process, deposition due to vegetation is absent and reductions are driven by dispersion only. A solid barrier with vegetation cover (Case 3, Fig. 5b) is found to behave very similar to the a solid barrier-only case. The additional particle reduction by having vegetation cover on a solid barrier is insignificant because the total leaf surface area of the cover is small compared to tree stands. A vegetation–solid barrier combination (Case 4, Fig. 5c) results in the highest reduction in downwind particle concentrations among the six configurations evaluated, although modeling suggests a large elevation in on-road concentrations occur. Similar to Case 2, the upwind vegetation barrier in Case 5 (Fig. 6) elevates the on-road concentration by slowing down the on-road wind speed and reducing the dispersion. However, the degree of on-road concentration elevation strongly depends on the wind direction. More parallel winds relative to the road leads to less of an increase in on-road concentrations. In addition, unlike barrier width, our analysis suggests that increasing the barrier height above those modeled only has a minor impact on near-ground particle concentration.

This study has some limitations for roadside vegetation barrier design. First, no other structures and topographies which may have complicated the near-road dispersion besides the roadside barriers are considered in the model. Second, the results are based on coniferous evergreens and may not be applicable to broad-leaved trees or bushy plants. Third, there are uncertainties associated with parameters such as LAD profiles, dry deposition models, drag coefficient and meteorology conditions. For instance, unlike wind tunnel and CFD studies, the meteorology condition is stochastic in the real word. Depending on the magnitude of variation, the impact of the concentration reduction could vary. Therefore, specific results in the simulation, such as the percentage of concentration reduction and size of the different regimes may not be generalized. While the general trends and recommendations presented in this study provide insights for vegetation barrier designs, future implementation needs to take into account site-specific characteristics, given the complexity of urban landscapes.

Appendix A. Supplementary data

Supplementary data to this article can be found online at http://dx.doi.org/10.1016/j.scitotenv.2015.09.067.

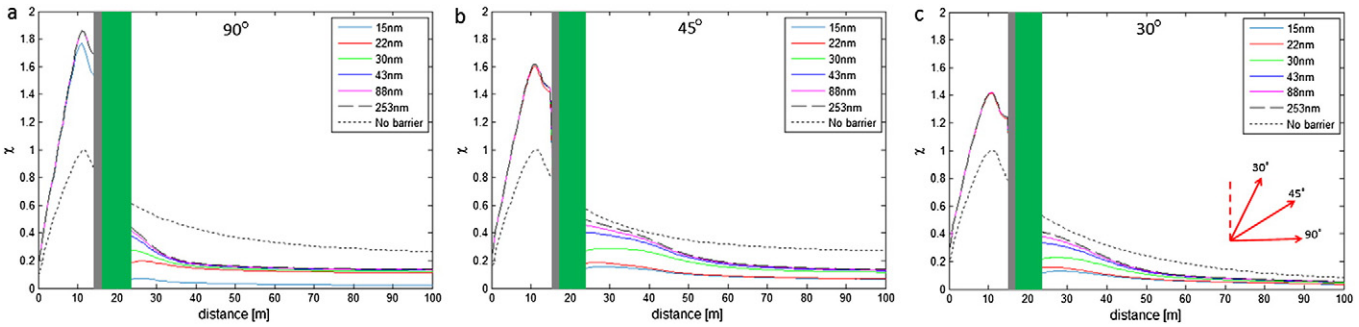

Fig. 9. Horizontal gradients of three oncoming wind directions: 30, 45, 90°. Wind direction of 90° is normal to the roadway.

References

Al-Dabbous, A.N., Kumar, P., 2014. The influence of roadside vegetation barriers on airborne nanoparticles and pedestrians exposure under varying wind conditions. Atmos. Environ. 90, 113–124.

Baldauf, R., Thoma, E., Khlystov, A., Isakov, V., Bowker, G., Long, T., et al., 2008. Impacts of noise barriers on near-road air quality. Atmos. Environ. 42, 7502–7507.

Baldauf, R., Jackson, L., Hagler, G., Vlad, I., McPherson, G., Nowak, D., et al., 2011. The Role of Vegetation in Mitigating Air Quality Impacts From Traffic Emissions.

Bowker, G.E., Baldauf, R., Isakov, V., Khlystov, A., Petersen, W., 2007. The effects of roadside structures on the transport and dispersion of ultrafine particles from highways. Atmos. Environ. 41, 8128–8139.

Brantley, H.L., Hagler, G.S.W., Deshmukh, P.J., Baldauf, R.W., 2014. Field assessment of the effects of roadside vegetation on near-road black carbon and particulate matter. Sci. Total Environ. 468–469, 120–129.

Cassiani, M., Katul, G.G., Albertson, J.D., 2008. The effects of canopy leaf area index on airflow across forest edges: large-eddy simulation and analytical results. Bound.-Layer Meteorol. 126, 433–460.

Dupont, S., Brunet, Y., 2008. Influence of foliar density profile on canopy flow: a large-eddy simulation study. Agric. For. Meteorol. 148, 976–990.

Finn, D., Clawson, K.L., Carter, R.G., Rich, J.D., Eckman, R.M., Perry, S.G., et al., 2010. Tracer studies to characterize the effects of roadside noise barriers on near-road pollutant dispersion under varying atmospheric stability conditions. Atmos. Environ. 44, 204–214.

Fuller, M., Bai, S., Eisinger, D., Niemeier, D., 2009. Practical Mitigation Measures for Diesel Particulate Matter: Near-road Vegetation Barriers. Contract AQ-04-01: Developing Effective and Quantifiable Air Quality Mitigation Measures. University of California, Davis.

Germano, M., Piomelli, U., Moin, P., Cabot, W.H., 1991. A dynamic subgrid-scale eddy viscosity model. Phys. Fluids A (1989–1993) 3, 1760–1765.

Hagler, G.S.W., Tang, W., Freeman, M.J., Heist, D.K., Perry, S.G., Vette, A.F., 2011. Model evaluation of roadside barrier impact on near-road air pollution. Atmos. Environ. 45, 2522–2530.

Hagler, G.S., Lin, M.-Y., Khlystov, A., Baldauf, R.W., Isakov, V., Faircloth, J., et al., 2012. Field investigation of roadside vegetative and structural barrier impact on near-road ultrafine particle concentrations under a variety of wind conditions. Sci. Total Environ. 419, 7–15.

Heist, D.K., Perry, S.G., Brixey, L.A., 2009. A wind tunnel study of the effect of roadway configurations on the dispersion of traffic-related pollution. Atmos. Environ. 43, 5101–5111.

Litschke, T., Kuttler, W., 2008. On the reduction of urban particle concentration by vegetation—a review. Meteorol. Z. 17, 229–240.

Lovett, G.M., 1994. Atmospheric deposition of nutrients and pollutants in North America: an ecological perspective. Ecol. Appl. 4, 630–650.

McDonald, A.G., Bealey, W.J., Fowler, D., Dragosits, U., Skiba, U., Smith, R.I., et al., 2007. Quantifying the effect of urban tree planting on concentrations and depositions of PM10 in two UK conurbations. Atmos. Environ. 41, 8455–8467.

Petroff, A., Zhang, L., Pryor, S.C., Belot, Y., 2009. An extended dry deposition model for aerosols onto broadleaf canopies. J. Aerosol Sci. 40, 218–240.

Pope, S.B., 2000. Turbulent Flows. Cambridge University Press.

Shaw, R.H., Schumann, U., 1992. Large-eddy simulation of turbulent flow above and within a forest. Bound.-Layer Meteorol. 61, 47–64.

Shaw, R.H., Zhang, X.J., 1992. Evidence of pressure-forced turbulent flow in a forest. Bound.-Layer Meteorol. 58, 273–288.

Steffens, J.T., Wang, Y.J., Zhang, K.M., 2012. Exploration of effects of a vegetation barrier on particle size distributions in a near-road environment. Atmos. Environ. 50, 120–128.

Steffens, J.T., Heist, D.K., Perry, S.G., Zhang, K.M., 2013. Modeling the effects of a solid barrier on pollutant dispersion under various atmospheric stability conditions. Atmos. Environ. 69, 76–85.

Steffens, J.T., Heist, D.K., Perry, S.G., Isakov, V., Baldauf, R.W., Zhang, K.M., 2014. Effects of roadway configurations on near-road air quality and the implications on roadway designs. Atmos. Environ. 94, 74–85.

Stull, R.B., 1988. An Introduction to Boundary Layer Meteorology vol. 13. Springer Science & Business Media.

Su, H.-B., Shaw, R., Paw, K., Moeng, C.-H., Sullivan, P., 1998. Turbulent statistics of neutrally stratified flow within and above a sparse forest from large-eddy simulation and field observations. Bound.-Layer Meteorol. 88, 363–397.

Thom, A., 1972. Momentum, mass and heat exchange of vegetation. Q. J. R. Meteorol. Soc. 98, 124–134.

Tominaga, Y., Mochida, A., Yoshie, R., Kataoka, H., Nozu, T., Yoshikawa, M., et al., 2008. AIJ guidelines for practical applications of CFD to pedestrian wind environment around buildings. J. Wind Eng. Ind. Aerodyn. 96, 1749–1761.

Tong, Z., Zhang, K.M., 2015. The near-source impacts of diesel backup generators in urban environments. Atmos. Environ. 109, 262–271.

Tong, Z., Wang, Y.J., Patel, M., Kinney, P., Chrillrud, S., Zhang, K.M., 2012. Modeling spatial variations of black carbon particles in an urban highway-building environment. Environ. Sci. Technol. 46, 312–319.

Wang, Y.J., Zhang, K.M., 2009. Modeling near-road air quality using a computational fluid dynamics model, CFD-VIT-RIT. Environ. Sci. Technol. 43, 7778–7783.

Wang, Y.J., Zhang, K.M., 2012. Coupled turbulence and aerosol dynamics modeling of vehicle exhaust plumes using the CTAG model. Atmos. Environ. 59, 284–293.

Wang, Y.J., DenBleyker, A., McDonald-Buller, E., Allen, D., Zhang, K.M., 2011. Modeling the chemical evolution of nitrogen oxides near roadways. Atmos. Environ. 45, 43–52.

Wang, Y.J., Yang, B., Lipsky, E.M., Robinson, A.L., Zhang, K.M., 2013a. Analyses of turbulent flow fields and aerosol dynamics of diesel engine exhaust inside two dilution sampling tunnels using the CTAG model. Environ. Sci. Technol. 47, 889–898.

Wang, Y.J., Nguyen, M.T., Steffens, J.T., Tong, Z., Wang, Y., Hopke, P.K, et al., 2013b. Modeling multi-scale aerosol dynamics and micro-environmental air quality near a large highway intersection using the CTAG model. Science of The Total Environment 443, 75–386.

Watanabe, T., 2004. Large-eddy simulation of coherent turbulence structures associated with scalar ramps over plant canopies. Bound.-Layer Meteorol. 112, 307–341.

Wilson, N.R., Shaw, R.H., 1977. A higher order closure model for canopy flow. J. Appl. Meteorol. 16, 1197–1205.

Zhang, K.M., Wexler, A.S., 2002. Modeling the number distributions of urban and regional aerosols: theoretical foundations. Atmos. Environ. 36, 1863–1874.

Zhang, L., Gong, S., Padro, J., Barrie, L., 2001. A size-segregated particle dry deposition scheme for an atmospheric aerosol module. Atmos. Environ. 35, 549–560.

Zhang, K.M., Wexler, A.S., Niemeier, D.A., Zhu, Y.F., Hinds, W.C., Sioutas, C., 2005. Evolution of particle number distribution near roadways. Part III: Traffic analysis and on-road size resolved particulate emission factors. Atmos. Environ. 39, 4155–4166.